Received: 2 November 2020 | Revised: 16 December 2020 | Accepted: 18 December 2020

DOI: 10.1111/cts.12975

ARTICLE

Hybrid physiologically-based pharmacokinetic model for remdesivir: Application to SARS-CoV-2

James M. Gallo

Department of Pharmaceutical Sciences, University at Buffalo, Buffalo, New York, USA

Correspondence
James M. Gallo, Department of Pharmaceutical Sciences, School of Pharmacy and Pharmaceutical Sciences, University at Buffalo, Buffalo, NY 14203, USA.
Email: jmgallo@buffalo.edu

Funding information
No funding was received for this work.

Abstract

A novel coronavirus, severe acute respiratory syndrome-coronavirus 2 (SARS-CoV-2) or coronavirus disease 2019 (COVID-19), has caused a pandemic that continues to cause catastrophic health and economic carnage and has escalated the identification and development of antiviral agents. Remdesivir (RDV), a prodrug and requires intracellular conversions to the active triphosphate nucleoside (TN) has surfaced as an active anti-SARS-CoV-2 drug. To properly design therapeutic treatment regimens, it is imperative to determine if adequate intracellular TN concentrations are achieved in target tissues, such as the lungs. Because measurement of such concentrations is unrealistic in patients, a physiologically-based pharmacokinetic (PBPK) model was developed to characterize RDV and TN disposition. Specifically, a hybrid PBPK model was developed based on previously reported data in humans. The model represented each tissue as a two-compartment model—both extracellular and intracellular compartment wherein each intracellular compartment contained a comprehensive metabolic model to the ultimate active metabolite TN. Global sensitivity analyses and Monte-Carlo simulations were conducted to assess which parameters and how highly sensitive ones impacted peripheral blood mononuclear cells and intracellular lung TN profiles. Finally, clinical multiple-dose regimens indicated that minimum lung intracellular TN concentrations ranged from ~ 9 uM to 4 uM, which suggest current regimens are effective based on in vitro half-maximal effective concentration values. The model can be used to explore tissue drug disposition under various conditions and regimens, and expanded to pharmacodynamic models.

Study Highlights

WHAT IS THE CURRENT KNOWLEDGE ON THE TOPIC?

There is limited information on the tissue distribution and metabolism of remdesivir (RDV)—an antiviral agent recently US Food and Drug Administration (FDA)-approved for patients with severe acute respiratory syndrome-coronavirus 2 (SARS-CoV-2)—and none in the patients.

WHAT QUESTION DID THIS STUDY ADDRESS?

RDV is known to undergo intracellular conversion to an active triphosphate nucleoside (TN) metabolite, and the computational investigation used a physiologically-based

This is an open access article under the terms of the Creative Commons Attribution-NonCommercial License, which permits use, distribution and reproduction in any medium, provided the original work is properly cited and is not used for commercial purposes.
© 2021 The Authors. *Clinical and Translational Science* published by Wiley Periodicals LLC on behalf of the American Society for Clinical Pharmacology and Therapeutics.

pharmacokinetic (PBPK) of RDV to characterize the tissue distribution of RDV and the intracellular metabolite kinetics and the production of TN.

WHAT DOES THIS STUDY ADD TO OUR KNOWLEDGE?

The PBPK model of RDV characterizes the extent of RDV tissue distribution and the associated intracellular metabolism in target tissues, such as the lungs. The model simulations can be used to assess the efficacy of current clinical dosing regimens based on TN intracellular concentration profiles.

HOW MIGHT THIS CHANGE CLINICAL PHARMACOLOGY OR TRANSLATIONAL SCIENCE?

The PBPK model of RDV serves as a foundation to rationally design clinical dosing protocols for RDV and may be extended to viral dynamic and pharmacodynamic models, and further support the development of PBPK models for other antivirals used for SARS-CoV-2.

INTRODUCTION

The global pandemic caused by severe acute respiratory syndrome-coronavirus 2 (SARS-CoV-2) has initiated a tremendous response from the scientific community to develop a vaccine and antiviral drugs. The discovery of new drugs specific for SARS-CoV-2 will take more time than repurposing drugs, many already US Food and Drug Administration (FDA) approved. There has been a large number of repurposed drugs from different therapeutic areas that have been proposed based primarily on in vitro antiviral activity.[1–3] How these drugs are used to treat patients with SARS-CoV-2 will likely be based on existing dosing protocols—at least initially—used in the diseases the drugs were developed for originally.[4] There is a role for pharmacokinetic (PK) and pharmacodynamic (PD) models to compare and contrast dosing recommendations based on metrics that can be predicted or simulated from the models as a means to define more efficacious treatments.[5–8] PK/PD models and extensions to viral dynamic models provide a rich set of platforms that can expeditiously deploy information that may benefit patients.[9,10]

Within the PK/PD modeling armamentarium, physiologically-based PK (PBPK) and PBPK/PD models offer tissue-specific and cell type-specific information that may be immensely beneficial to design drug treatments because target site drug concentrations can be predicted and used as metrics to design drug dosing regimens.[11–14] Moreover, PBPK and PBPK/PD models provide mechanistic details that are valuable to understand nuanced characteristics of drug action, provide a strong rationale to design drug combinations therapies, and adapt to the evolution of the virus as it mutates, and already observed for SARS-CoV-2.

Remdesivir (RDV) is an antiviral drug originally developed for Ebola and now being used in patients with SARS-CoV-2,[15–18] and recently FDA-approved.[19] It inhibits RNA-dependent RNA polymerase (RdRp) that ultimately prevents viral replication.[20] The purpose of this investigation was to develop a PBPK model for RDV, assess current regimens being used in patients with SARS-CoV-2, and how it may be refined and extended to design drug therapy in patients.

MATERIALS AND METHODS

Basic characteristics of the hybrid PBPK model for RDV

The model was constructed in part from human data that primarily consisted of plasma concentrations measurements of RDV (remdesivir, GS-5734), A (alanine metabolite, GS-704277), and N (nucleoside metabolite, GS-441524) reported for nine human cohorts.[21] The prior report[21] also contained data on the active triphosphate nucleoside (TN) as did the request for compassionate use in the European Union.[22] All concentration-time series data was digitized using the Un-Scan-It software.[23]

A forcing function model was derived from the available plasma concentrations and PK metrics recently reported.[21] RDV, A and N metabolite plasma concentrations were measured in 9 cohorts of healthy subjects as single doses of RDV from 3 mg to 225 mg administered as either 0.5 or 2-h constant rate intravenous (i.v.) infusions, as well as in a multiple-dose regimen cohort that received 150 mg as a 1-h i.v. infusion. Specifically, digitized plasma concentration-time measurements in five (4 single-dose cohorts and day 1 of the multiple-dose cohort) of the seven cohorts and reported peak plasma concentration (C_{max}) and area under the drug concentration-time curve from time 0 to the last measured value or the last quantifiable concentration ($AUC_{0–last}$) values in an additional three additional cohorts were used to derive the forcing function model. Data from 2 single-dose cohorts were not used; the measurements in cohort 1 at the lowest 3 mg dose did not provide an estimate of clearance because RDV concentrations were below detection for much of the sampling period, and the data from cohort 4 (75 mg dose)

were inconsistent with the other cohorts due to long terminal phase measurements. A sequential approach was used in which a two-compartment model was first fit to the RDV plasma concentrations and AUC values, followed by fitting models for A and N metabolites. Maximum likelihood estimation with an additive error model was applied at each step. A linear two-compartment model was applied to the RDV measurements, whereas both the A and N metabolite models consisted of a first-order conversion (RDV to A, and A to N) and an elimination rate constant for each metabolite. This parsimonious forcing function model for RDV, A and N was then used in the PBPK model.

It is important to appreciate the intracellular metabolism of RDV[15,16,24] (see Figure 1) that is the cornerstone of the PBPK model. The metabolism of RDV has been determined in vitro in multiple cell types including HeLa cells, primary human and rhesus monkey peripheral blood mononuclear cells, human lung epithelial cells (Calu-3 2B4), and in the lungs of *Ces1c*$^{-/-}$ mice and marmosets confirming the major TN metabolite.[15,16] It can be seen that RDV, a Sp isomer of the 2-ethylbutyl-L-alanine phosphoramidate prodrug, undergoes a multistep reaction to produce the TN (also known as GS-443902) intracellularly, the active moiety that inhibits viral replication through RdRp. The multistep metabolic reactions are attributed to esterases, a phosphoamidase-type enzyme and host cell kinases and phosphatases.[24] The nucleoside metabolite, often referred to as Nuc (N) was developed as a parent antiviral agent and is generated from RDV via a monophosphate nucleoside (see Figure 1), although the conversion of Nuc to TN is slower than RDV.[15,24] The metabolism of RDV is not confined to plasma and the liver and is attributed to hydrolases throughout the body and subsequent conversions with kinases.[22,24] The metabolic scheme shown in Figures 1 and 2 is preserved in all tissue compartments.

It was assumed that only RDV and N could transport from the extracellular to intracellular compartments because the charged species would unlikely penetrate the cell membranes.[24] The unbound fraction of RDV in human plasma has been reported as 0.12 and N within the range of 1. These values were used in mass transport flux equations as shown below:

$$n_x^{\text{ecic}} = t\text{CL}_x \left(C_p^u - C_x^u \right)$$

where n_x^{ecic} = flux from the extracellular to intracellular compartment in tissue x, amount/time

$$t\text{CL}_x = \text{transport clearance tissue } x, \frac{\text{volume}}{\text{time}}$$

$$C_p^u = \text{unbound plasma concentration}, \frac{\text{amount}}{\text{volume}}$$

$$C_x^u = \text{unbound concentration in tissue } x, \frac{\text{amount}}{\text{volume}}$$

Substitute in for the unbound concentration and rewrite as:

$$n_x^{\text{ecic}} = t\text{CL}_x \left(f_u^p C_p - f_u^x C_x \right)$$

where

$$f_u^p = \text{fraction unbound in plasma}$$

$$f_u^x = \text{fraction unbound in tissue } x$$

$$C_p = \text{total plasma concentration}$$

$$C_x = \text{total concentration in tissue } x$$

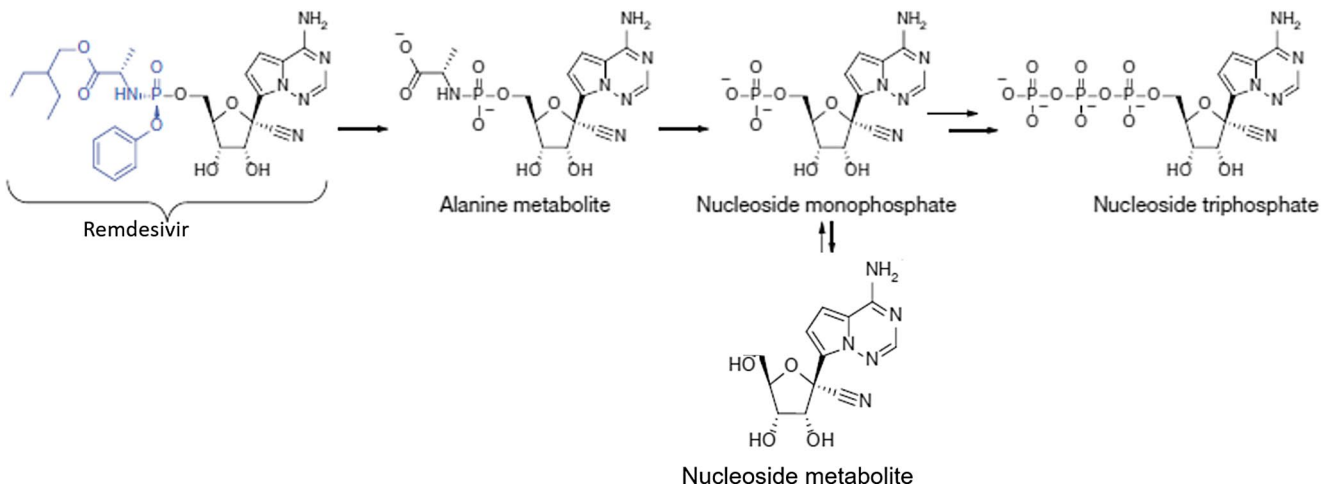

FIGURE 1 Primary cellular metabolism of remdesivir. Notice the reversible reaction between nucleoside monophosphate (MP in the text) and the nucleoside metabolite (N in the text). Addition of the functional group (blue) to remdesivir accelerates its conversion to the nucleoside triphosphate (TP in the text) compared with the conversion from N. Adapted from Warren et al.[15]

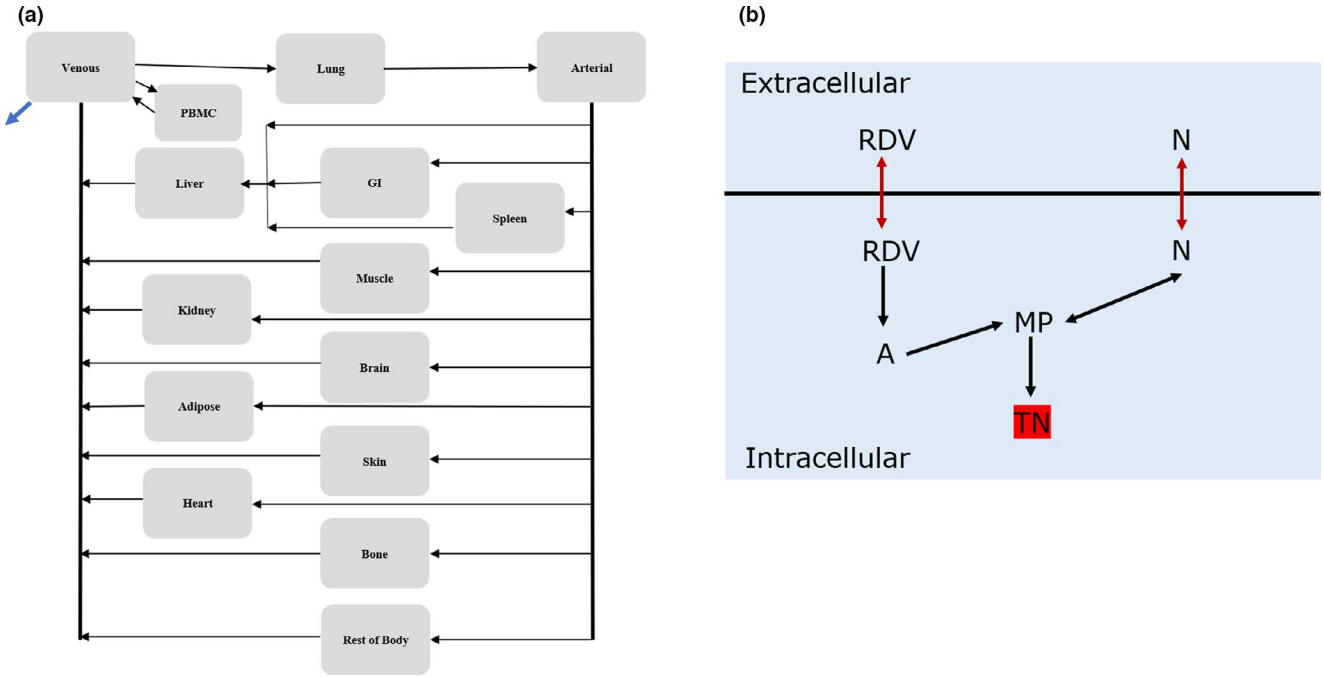

FIGURE 2 Physiologically-based pharmacokinetic model (PBPK) for RDV. (a) The whole-body structure. (b) Representation of extracellular-intracellular structure used for each tissue. Red bidirectional arrows indicate membrane transport, whereas black arrows indicate metabolism. A, alanine metabolite; RDV, remdesivir; MP, nucleoside monophosphate; N, nucleoside; TN, triphosphate nucleoside

Define

$$R_x = \frac{f_u^p}{f_u^x}$$

where R_x = partition coefficient in tissue x

Now rewrite the transport equation as:

$$n_x^{\text{ecic}} = t\text{CL}_x f_u^p \left(C_p - \frac{C_x}{R_x} \right)$$

This flux equation applies to both RDV and N and was used in all tissues. The main assumption is that the unbound fraction of RDV and N in plasma is equal to the unbound fraction in the extracellular compartment.

Parameters for the PBPK model for RDV

Organ plasma flow rates and tissue compartment volumes were obtained from PK-Sim[25] based on the characteristics of a normal White adult male with a body weight of 80 kg (specified as Nhanes, 1997). A hematocrit of 0.45 was assumed to convert blood to plasma flow rates and to correct vascular blood volumes to plasma volumes. In silico estimation of tissue partition coefficients that rely on aqueous solubility, p*K*a values, log octanol:water partition coefficients, and the unbound fractions in plasma for both RDV and N were based on the PK-Sim[25] default method, reported as the intracellular:plasma partition coefficient.

The intracellular metabolic kinetics (see Figure 2) was based on the sparse peripheral blood mononuclear cell (PBMC) TN data previously reported.[21,22] This data consisted of maximum and 24-h postdose TN PBMC concentrations and the AUC to the last sampling time for different cohorts administered RDV at doses from 75 mg to 200 mg and i.v. infusion times of 0.5 and 2 h. Rather than estimate the very small volume of PBMCs and introduce unnecessary error, first-order rate constants (h^{-1}) were assumed for each metabolic conversion that enabled concentration rate equations to be used. The values of the rate constants were obtained iteratively and then converted to metabolic clearances for each tissue compartment where intracellular volumes were known and reported.[25]

Model performance based on reported data

The hybrid PBPK model of RDV was used to generate RDV, A and N plasma concentration-time profiles for each cohort with time-series data using 500 Monte-Carlo simulations. A 20% coefficient of variation (CV) in the parameters forming the forcing function model was used for the simulations. Comparisons between previously reported[21] observed model-predicted AUC and C_{max} values were also completed for all cohorts.

A Sobol global sensitivity analyses[26] with done using the PBMC parameters (10 parameters in total) as input and the TN AUC values as the output metric. Replicate runs of 100,000 samples were completed to assess reproducibility. Subsequently, of the 10 input parameters that showed appreciable sensitivity

indices (main effects > 0.1) were used in Monte-Carlo simulations to assess how 20% CV parameter variability impacted the TN PBMC AUC values and compared those predicted values with the observed values for different cohorts.

Multiple-dose regimens

Multiple-dose simulations were focused on understanding the determinants of lung intracellular TN concentrations as they are likely a key PD end point to evaluate clinical treatment schedules. An analogous strategy was used as for assessing TN PBMC concentrations. First, a global sensitivity analysis was done to identify which of the 10 lung intracellular parameters had high sensitivity coefficients based upon their impact on lung intracellular TN AUC values. Next, those sensitive parameters—with 20% CV—were used in Monte-Carlo simulations to predict lung intracellular TN concentrations following a standard multiple-dose regimen. The hybrid PBPK model was used to generate lung intracellular TN concentrations after multiple-dose schedules. Specifically, 2 regimens were used; both used a 200 mg loading dose followed by 4 daily 100 mg doses given as i.v. infusions using either a 1 or 2-h infusion time. Both regimens are standard schedules used to treat patients with coronavirus disease 2019 (COVID-19).

Computer software

All models were developed and run using Magnolia.[27] Magnolia uses advanced continuous simulation language and generates.csl files. The hybrid PBPK model consisted of 84 ordinary differential equations and 178 parameters. The sensitivity analyses were accessed using Windows scripts and the Monte-Carlo simulations via Python scripts, both directly from Magnolia. The main program code is available from GitHub (see Supplement).

RESULTS

Model performance based on reported data

Tables S1–S3 provides the model parameters for the forcing function model, the physiological parameters and RDV and N metabolite partition coefficients and transport parameters,

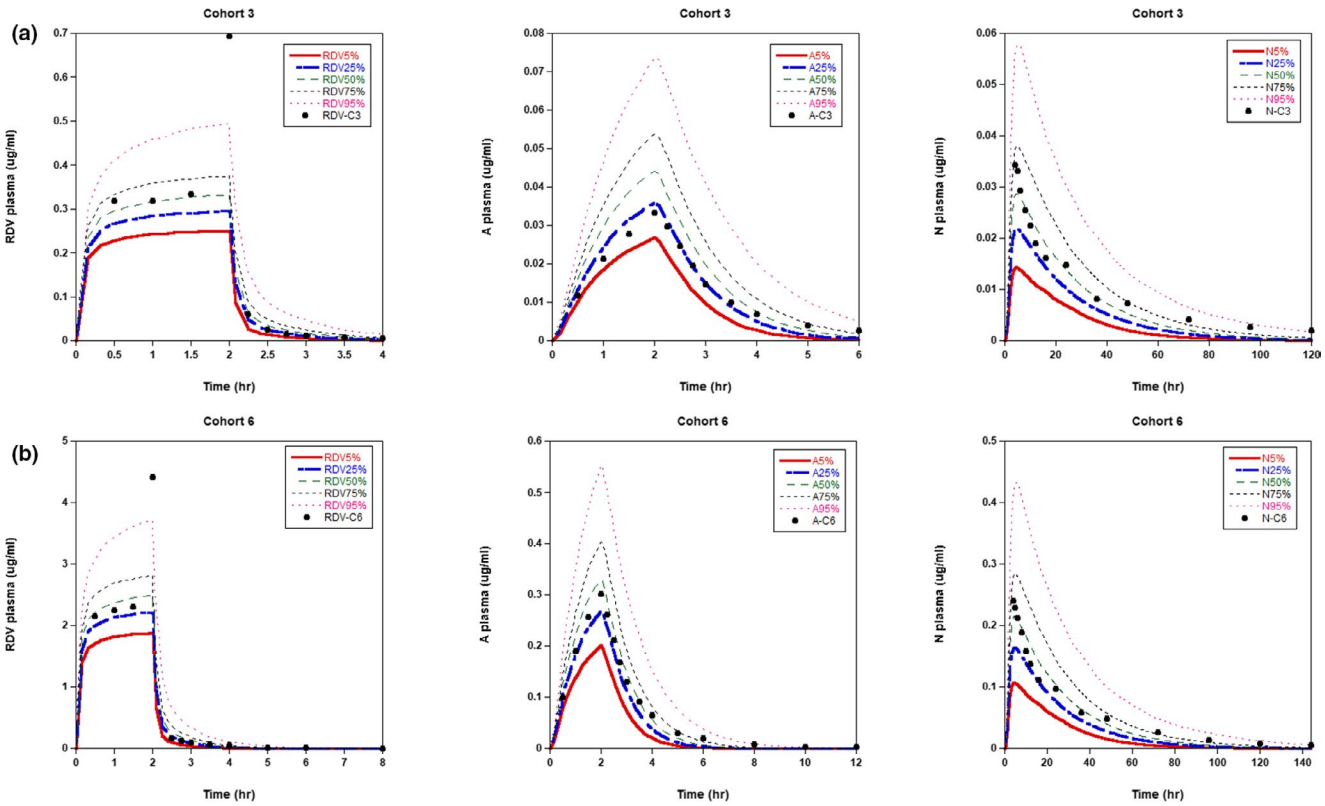

FIGURE 3 Hybrid PBPK model-predicted and reported plasma concentrations for RDV, A and N. (a) Cohort 3 (as referred to in reference 20) administered 30 mg of RDV as a 2-h i.v. infusion. (b) Cohort 6 administered 225 mg of RDV as a 2-h i.v. infusion. For each cohort, 500 Monte-Carlo simulations were done with 20% CV in the forcing function parameters that define the plasma kinetics. The lines represent the percentile bands—from 5% to 95%—based on the 500 simulations. The black circles represent the digitized plasma concentration for each species extracted from reference 20 that showed the mean measurements. CV, coefficient of variation; PBPK, physiologically-based pharmacokinetic; RDV, remdesivir

and the intracellular metabolic and elimination parameters, respectively.

To test the agreement between model-predicted and measured RDV, A and N plasma concentrations, Monte-Carlo simulations were completed with the hybrid PBPK model wherein 20% variability was used for all parameters in the forcing function model. Acceptable agreement was obtained for all patient cohorts that received RDV doses from 10 mg to 225 mg. Figure 3 illustrates the results for two representative cohorts (names assigned as reported in reference 20), cohort 3 a single 30 mg 2-h i.v. infusion and cohort 6 a single 225 mg 2-h i.v. infusion (see Figures S1–S2 in the Supplement for the remining cohorts). In all cohorts, the mean observed measurements typically fall within the 25–50% bands of the Monte-Carlo simulations. In cohorts 2, 3, and 6, the reported end of infusion RDV plasma concentrations were greater than even the 95% band and appear more as an aberration given the much lower concentrations during the infusion that are captured by the model. In addition, the percentage bias between model-predicted and reported AUC and C_{max} values (see Table 1), which included three additional cohorts, were less than 20% with most exceptions due to the high end of infusion RDV plasma C_{max} values. Nonetheless, even in these cases, the percentage bias in the AUC values were low.

The reported TN PBMC data that consisted of C_{max} and C24 concentrations and AUC values were key to the development of the intracellular model. As stated above, it was assumed that only RDV and the N metabolite could enter PBMCs. Once in the PBMCs, the complete metabolic scheme (see Figure 2) was modeled. The available observed data were sufficiently sparse that model optimizations were inconclusive, and thus, final values for the first-order rate constants were arrived at iteratively (Table S3). The percentage bias between model-predicted and reported PBMC TN concentrations and AUC values are given in Table 2. For three of the four cohorts, the percentage biases are 20% or less, and the large percentage bias for cohort 9 are difficult to explain because the only difference between RDV dosing between cohort 7 was the 75 mg dose was given as a 30-min infusion rather than a 2-h infusion. Under the condition of linearity, the AUC values should be equal. Without an actionable explanation, the model for the intracellular kinetics in PBMCs was deemed acceptable and underwent a global sensitivity analysis using all 10 associated parameters with the PBMC TN AUC as the output variable. It was found that the most sensitive parameters were the RDV transport rate constant between plasma and PBMCs, and the elimination rate constant for TN (see Figure S3). Based on these results, Monte-Carlo simulations were completed with the hybrid PBPK using 20% CV in the 2 sensitive parameters. It can be seen that the model-predicted time course of TN replicates the observed—yet limited—data well (see Figure 4).

TABLE 1 Percentage bias between model-predicted and measured plasma AUC and C_{max} values[a]

	RDV		A metabolite		N metabolite	
Cohort	AUC	C_{max}	AUC	C_{max}	AUC	C_{max}
2	−4.3	−50.2	23	21.7	28.7	6.7
3	−12.7	−52.4	19	29.4	−8.1	−17.6
5	14.4	−42.8	10.4	28.9	−9.3	−7.9
6	−4.9	−52.5	0	4.8	−12.7	−14.4
MC1	30.2	−9.1	−6.6	5	26.1	4.3
7	−7.1	−51.2	12.9	−3.5	0	−10.3
8	4	−37	−18.2	−6	−2.1	−5.4
9	34.4	3.4	−5.1	12.2	7.8	1.4

AUC, area under the drug concentration-time curve; C_{max}, peak plasma concentration; RDV, remdesivir.

[a]%Bias = (model-predicted-measured)/measured *100. All AUC values based on to last measured time point except for cohort MC1 (multiple-dose day 1) the AUC reported was from 0 to 24 h. All measured C_{max} and AUC values and cohort numbers are as reported by Humeniuk et al.[20] Cohort 7 received 75 mg of RDV as a 2-h i.v. infusion, cohort 8 150 mg of RDV as a 2-h infusion and cohort 9 75 mg of RDV as a 30-min infusion.

Multiple-dose regimens

Because measurements of lung concentrations for RDV and any of the metabolites were unavailable, a sensitivity analysis was completed to assess which model parameters impacted the active metabolite TN concentrations. Similar to the model for PBMCs, the transport clearance of RDV between the extracellular and intracellular lung compartments and the elimination clearance of TN were identified as significant factors (see Figure S4). Monte-Carlo simulation with 20% CV in these 2 parameters were completed using clinical regimens of RDV used in patients with COVID-19 (see Figures 5 and S4, 1-h and 2-h infusion times, respectively). Lung extracellular RDV concentrations, which serve

TABLE 2 Percentage bias between model-predicted and measured TN values[a]

Cohort	C_{max}	C24	AUC
7	16	−1.4	−3.4
8	−8.3	16.2	5.9
9	−50.8	−34.2	−57.3
T16	−20.4	−17.4	−0.01

AUC, area under the drug concentration-time curve; C_{max}, peak plasma concentration; RDV, remdesivir; TN, triphosphate nucleoside.

[a]%Bias = (model-predicted-measured)/measured *100. Measured C_{max}, C24, and AUC values and cohort numbers for 7, 8, and 9 are as reported by Humeniuk et al.[20] The values for cohort T16 (table 16) are from reference.[21] Cohort 7 received 75 mg of RDV as a 2-h i.v. infusion, cohort 8 150 mg of RDV as a 2-h infusion, and cohort 9 75 mg of RDV as a 30-min infusion. Cohort T16 received 200 mg RDV as a 30-min infusion.

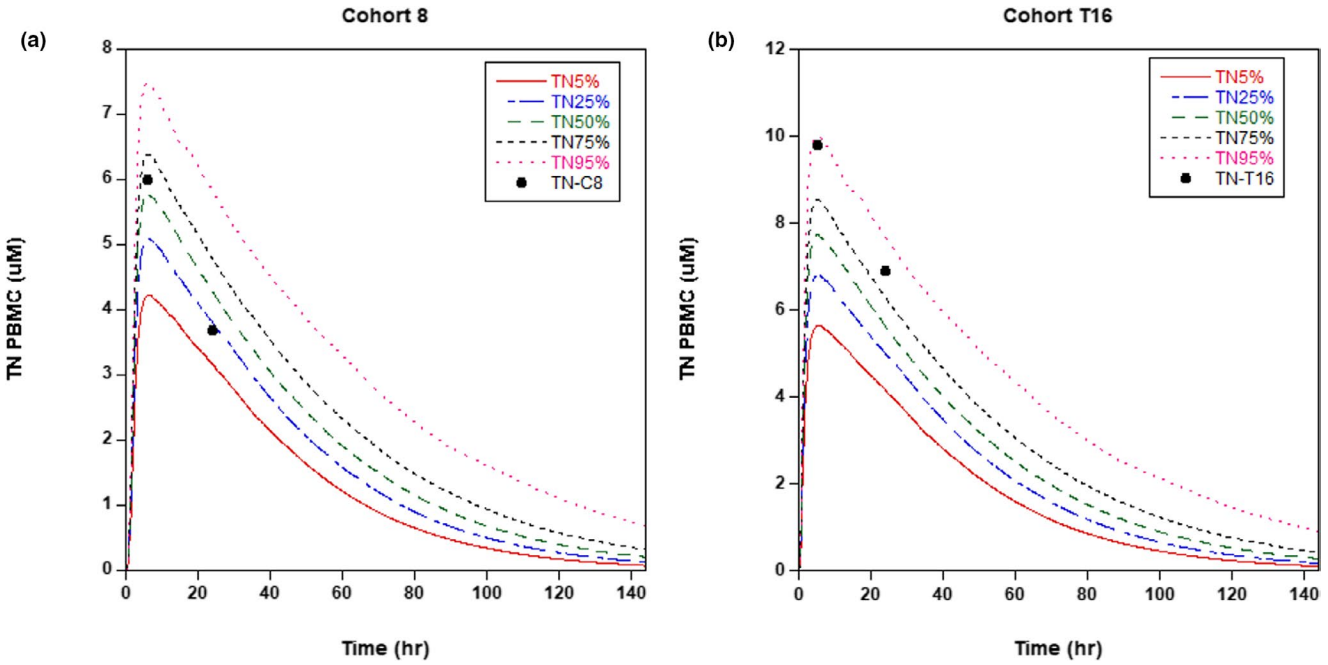

FIGURE 4 Hybrid PBPK model-predicted and reported PBMC triphosphate nucleoside (TN) concentrations. (a) Cohort 8 (as referred to in reference 20) administered 150 mg of RDV as a 2-h i.v. infusion. (b) Cohort T16 (from reference 21 see table 16) administered 200 mg of RDV as a 30-min i.v. infusion. For each cohort, 500 Monte-Carlo simulations were done with 20% CV in the RDV extracellular-intracellular transport rate constant (9.0 h^{-1}, see Tables 2 and 3) and the TN elimination rate constant (0.03, h^{-1}, see Table S3). The lines represent the percentile bands—from 5% to 95%—based on the 500 simulations. The black circles represent the mean TN PBMC concentration reported in references 20 (cohort 8) and 21 (cohort T16). CV, coefficient of variation; PBMC, peripheral blood mononuclear cell; PBPK, physiologically-based pharmacokinetic

as a metric to compare to in vitro cell data that yield effective concentrations, such as half-maximal effective concentration (EC_{50}) values,[28] are shown in Figure 5a, and corresponding TN lung intracellular concentrations in Figure 5b. RDV extracellular concentrations reach a C_{max} value of about 7 μM after the 200 mg loading dose and then are about 3.5 μM for the remaining four 100 mg doses. Regardless of the C_{max} value, RDV does not accumulate and is eliminated rapidly with lung extracellular concentrations falling below 0.1 μM at just over 2 h after the start of the infusions. Lung intracellular TN concentrations (Figures 5b and S5b) following either 1-h or 2-h infusion durations vary just over 2-fold over the 5-day course of therapy with steady-state minimum concentrations ranging from 4 μM to 9 μM at the 5% and 95% levels. The 2-h infusion duration delayed the time of the maximum lung intracellular TN C_{max} by an hour, from 5 to 6 h. Although in vitro efficacy data against SARS-CoV-2 vary depending on the experimental conditions, RDV EC_{50} values range from about 0.1–1 μM,[22,29] and suggest current clinical regimens should be effective.

DISCUSSION

There is a massive effort to repurpose drugs for SARS-CoV-2[30,31] and an indication drug therapy for COVID-19 will be part of the therapeutic armamentarium even in the event of an effective vaccine. RDV—a broad-spectrum antiviral agent—has surfaced as one of the more promising agents and has been recently granted FDA approval.[19]

Human PK data have started to emerge that highlight the rapid elimination of RDV, a prodrug, and essentially dose-independent PK behavior based on noncompartmental analyses of plasma concentration-time data.[21] Two metabolites, the A and N metabolites have also been measured in plasma of humans and show fairly constant metabolite/parent drug AUC ratios supporting linear PKs. Finally, the active metabolite, TN, has been measured in PBMCs that often serve as a surrogate for antiviral intracellular disposition, as done here. PBPK models are sought for their ability to predict tissue disposition,[12] both target and toxic sites, which is a powerful simulation tool to aid drug development and design effective dosing schedules. Lung concentrations of RDV and TN could be highly beneficial in this regard and provided the motivation for this project.

The efforts to devise a global PBPK model—without the use of the forcing function model—resulted in models that tended to underpredict RDV plasma concentrations, particularly at later times postinfusion. In addition, alanine metabolite plasma concentration-time profiles were very difficult to capture with a global approach; however, the plasma N metabolite concentrations could be captured reasonably well.

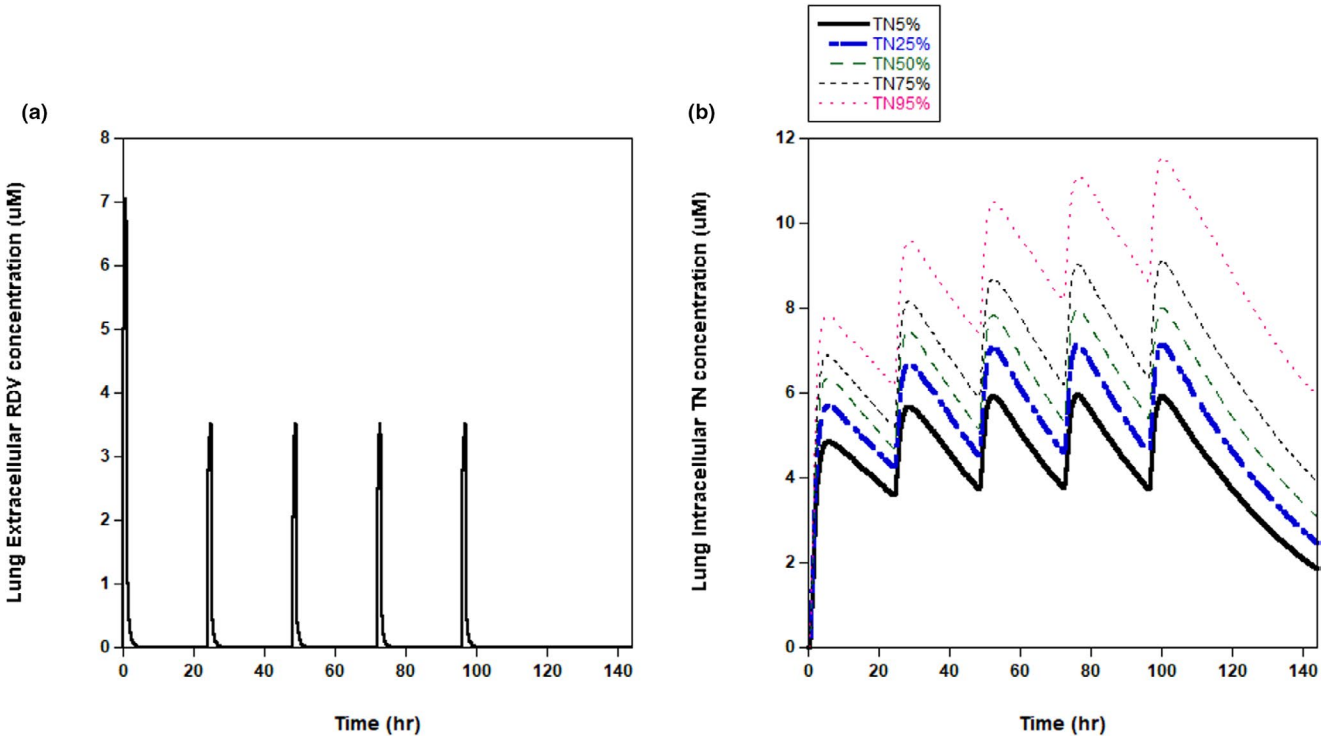

FIGURE 5 Multiple-dose hybrid PBPK model-simulated lung concentrations. (a) RDV lung extracellular compartment concentrations. (b) Triphosphate nucleoside (TN) lung intracellular concentrations. RDV was administered as a 1-h infusion each day and on day 1 the dose = 200 mg and on days 2–5 = 100 mg. Monte-Carlo simulations (n = 500) were done with 20% CV in the RDV lung extracellular-intracellular transport clearance (2.5 L/h, see Table 2) and the lung elimination clearance of TN (0.0084 L/h, see Table S3). In (b), the lines represent the percentile bands—from 5% to 95%—based on the 500 simulations, whereas in (a) the single line is equivalent for each of the 500 simulations because neither parameter effects the extracellular RDV concentrations. PBPK, physiologically-based pharmacokinetic; RDV, remdesivir

Part of the difficulty in developing a metabolic model to describe the plasma profiles of RDV and the metabolites is the uncertain potential of kinases and phosphatases to act in plasma, and thus, play a role in the reversible reaction between the monophosphate nucleoside and the N metabolite (Figure 1). Without dephosphorylation and phosphorylation reactions—normally considered intracellular—occurring in plasma, A plasma concentrations were seemingly dependent on carrier-mediated efflux from tissues to better replicate the plasma concentration-time profile. Therefore, the forcing function approach was a reasonable approach to characterize the available plasma measurements, and a method we have previously used in PBPK models.[32,33] The forcing function model parameters for total systemic clearance and apparent volume of distribution for RDV agreed with values reported[21] and only required two additional parameters for each of the A and N metabolites, a formation rate, and an elimination rate constant. As shown in Figures 3 and S1–S2, incorporation of the forcing function model into the PBPK model yielded suitable prediction of all measured plasma species.

The intracellular metabolic model that coincided with the scheme shown in Figure 1 was based on PBMC TN concentration measurements previously reported, and consisted of C_{max}, C24, and AUC values from four cohorts.[21,22] It is known from in vitro cell studies that the conversion of RDV to TN is much faster and more efficient than from the N metabolite.[15] These data and combined with the assumption that only RDV and N were transported into intracellular compartments simplified the development of the PBMC intracellular model (Figure 2b). The RDV plasma-PBMC transport rate was nine times that of the N metabolite and consistent with other reports based on cell data.[24] The metabolic rate constants for RDV to A conversion and the monophosphate to the TN moiety were the highest, being about 10-fold greater than the remaining metabolic rate constants (Table S3). The PBMC model was parameterized in terms of species concentrations since the volume estimates of the PBMC compartment were variable, and would, accordingly, have a large impact on concentrations given its relatively very small volume. Moreover, by defining PBMC kinetic parameters in terms of first-order rate constants provided a simple means to scale parameters—transport and metabolic clearances (Tables S2 and S3)—to all other tissues by using their intracellular volumes that are more certain and tabulated.[25] The hybrid PBPK model-predicted PBMC TN concentrations agreed well with the reported values for three of the four cohorts (see above).

The multiple-dose administrations centered on predictions of lung intracellular TN concentrations as this is a target

tissue for COVID-19. The sensitivity analysis identified the RDV extracellular-intracellular transport clearance and the TN elimination clearance as highly impactful (Figure S4) and similar to that found for PBMCs. Monte-Carlo simulations with 20% CV in these 2 parameters for standard treatment regimens indicate RDV lung extracellular concentrations achieve values above in vitro-based EC_{50} values at least for a few hours. As expected, the shorter duration of the i.v. infusion—1 h (Figure 5a) vs. 2 h (Figure S5A)—proportionately affects the C_{max} values, but not the total exposure given the equivalent total doses. Interestingly, TN profiles are minimally affected by a 1-h change in the RDV infusion time (compare Figures 5b and S5B), and, as expected, reached higher concentrations and had a prolonged residence in the lung intracellular compartment than RDV concentrations. A recent investigation using a viral dynamic model indicated that the EC_{50} concentrations may be inadequate to assess efficacy and preferred effective concentration 90% (EC_{90}) concentrations.[10]

The hybrid PBPK model would benefit from tissue concentration-time data and studies to explore carrier-mediated transport. RDV is reported[22] to be a substrate for OAT1B1, OAT1B2, and P-glycoprotein but the kinetics of these reactions have not been reported, and thus, inclusion of these processes in the disposition of RDV is currently unjustified. The A and N metabolites are reported[22] not to be OAT1 and 3 substrates, but detailed studies would be definitive.

The current hybrid PBPK model suggests clinical treatment schedules are achieving effective target site concentrations, at least based on EC_{50} values. The recent FDA approval[19] based on clinical efficacy data also support the current dosing paradigms. Whether and how extensively SARS-CoV-2 mutates to resistance clones remains to be determined, but in vitro resistance investigations have found up to fivefold resistance to RDV conferred by mutations in the target enzyme, RdRp.[20] A similar extent of RDV resistance to SARS-CoV-2 would likely limit efficacy using the current RDV regimens as a single agent. The previously mentioned viral dynamic model[10] indicated that initiation and timing of RDV are important to viral control and certainly such models can be linked to the hybrid PBPK model that could lead to a strong basis to design optimal therapeutic regimens. Nonetheless, the current hybrid PBPK model serves as a tool to explore alternate dosing schedules based on PK metrics, and a foundation to develop more sophisticated viral dynamic and PD models.

ACKNOWLEDGMENT

I thank Conrad Housand of Magnolia Sciences for valuable input on coding and scripting.

CONFLICT OF INTEREST

The authors declared no competing interests for this work.

AUTHOR CONTRIBUTIONS

J.G. wrote the manuscript, designed the research, performed the research, and analyzed the data.

REFERENCES

1. Barlow A, Landolf KM, Barlow B, et al. Review of emerging pharmacotherapy for the treatment of coronavirus disease 2019. *Pharmacotherapy*. 2020;40:416-437.
2. Sanders JM, Monogue ML, Jodlowski TZ, Cutrell JM. Pharmacologic treatments for coronavirus disease 2019 (COVID-19): A review. *JAMA*. 2020;323:1824-1836.
3. Martinez MA. Clinical trials of repurposed antivirals for SARS-CoV-2. *Antimicrob. Agents Chemother*. 2020;64:e01101-e1120.
4. Tu YF, Chien CS, Yarmishyn AA, et al. A review of SARS-CoV-2 and the ongoing clinical trials. *Int J Mol Sci*. 2020;21:2657.
5. Zhou Q, Gallo JM. The pharmacokinetic/pharmacodynamic pipeline: Translating anticancer drug pharmacology to the clinic. *AAPS J*. 2011;13:111-120.
6. Yao X, Ye F, Zhang M, et al. In vitro antiviral activity and projection of optimized dosing design of hydroxychloroquine for the treatment of severe acute respiratory syndrome coronavirus 2 (SARS-CoV-2). *Clin Infect Dis*. 2020;71:732-739.
7. Verscheijden LFM, Zanden TM, Bussel LPM, et al. Chloroquine dosing recommendations for pediatric COVID-19 supported by modeling and simulation. *Clin Pharmacol Ther*. 2020;108:248-252.
8. Rowland-Yeo K, Zhang M, Pan X, et al. Impact of disease on plasma and lung exposure of chloroquine, hydroxychloroquine and azithromycin: Application of PBPK modeling. *Clin Pharmacol Ther*. 2020;108:976-984.
9. Hill AL, Rosenbloom DIS, Nowak MA, Siliciano RF. Insight into treatment of HIV infection from viral dynamics models. *Immuno Rev*. 2018;285:9-25.
10. Gonçalves A, Bertrand J, Ke R, et al. Timing of antiviral treatment initiation is critical to reduce SARS-CoV-2 viral load. *CPT Pharm Syst*. 2020;9:509-514.
11. Rowland M, Peck C, Tucker G. Physiologically-based pharmacokinetics in drug development and regulatory science. *Annul Rev Pharmacol Tox*. 2011;51:45-73.
12. Guo Y, Chu X, Parrott NJ, et al. Advancing predictions of tissue and intracellular drug concentrations using in vitro, imaging and physiologically based pharmacokinetic modeling approaches. *Clin Pharmacol Ther*. 2018;104:865-889.
13. Ballesta A, Zhou Q, Zhang X, Lv H, Gallo JM. Multiscale design of cell-type-specific pharmacokinetic/pharmacodynamic models for personalized medicine: Application to temozolomide in brain tumors. *CPT Pharm Syst Pharmacol*. 2014;3:e112.
14. Lukacova V, Goelzer P, Reddy M, Greig G, Reigner B, Parrott N. A physiologically based pharmacokinetic model for ganciclovir and its prodrug valganciclovir in adults and children. *AAPS J*. 2016;18:1453-1463.
15. Warren TK, Jordan R, Lo MK, et al. Therapeutic efficacy of the small molecule GS-5734 against Ebola virus in rhesus monkeys. *Nature*. 2016;531:381-385.
16. Sheahan TP, Sims AC, Graham RL, et al. Broad-spectrum antiviral GS-5734 inhibits both epidemic and zoonotic coronaviruses. *Sci. Trans. Med*. 2017;9:eaal3653.
17. Yang C-J, Wei Y-J, Chang H-L, et al. Remdesivir use in the coronavirus disease 2019 pandemic: A mini-review. *J Microbiol Immunol Infect.* https://doi.org/10.1016/j.jmii.2020.09.002.

18. Beigel JH, Tomashek KM, Dodd LE, et al. Remdesivir for the treatment of Covid-19 – final report. *N Engl J Med*. 2020;383(19):1813-1826.
19. Rubin D, Chan-Tack K, Farley J, et al. FDA approval of remdesivir – a step in the right direction. *N Engl J Med*. 2020;383(27): 2598-2600.
20. Agostini ML, Andres EL, Sims AC, et al. Coronavirus susceptibility to the antiviral remdesivir (GS-5734) is mediated by the viral polymerase and the proofreading exoribonuclease. *MBio*. 2018;9:e00221-e318.
21. Humeniuk R, Mathias A, Cao H, et al. Safety, tolerability, and pharmacokinetics of remdesivir, an antiviral for treatment of COVID-19. *Healthy Subjects Clin Transl Sci*. 2020;13:896-906.
22. European Medicines Agency. Summary of compassionate use. Remdesivir Gilead. Procedure No. EMEA/H/K/5622/CU. April 3, 2020.
23. Un-Scan-It, Graph Digitizing Software, version 7. Silk Scientific Corporation, <https://www.silkscientific.com/graph-digitizer.htm>.
24. Eastman RT, Roth JS, Brimacombe KR, et al. Remdesivir: A review of its discovery and development leading to emergency use authorization for treatment of COVID-19. *ACS Cent Sci*. 2020;6:672-683.
25. Pk-Sim®, version 8. Open Systems Pharmacology <http://www.open-systems-pharmacology.org/>.
26. Zhang XY, Trame MN, Lesko LJ, Schmidt S. Sobol sensitivity analysis: A tool to guide the development and evaluation of systems pharmacology models. *CPT Pharmacometrics Syst Pharmacol*. 2015;4:69-79.
27. Magnolia, version 1.3.9. <https://www.magnoliasci.com/>.
28. Fan J, Zhang X, Liu J, et al. Connecting hydroxychloroquine in vitro antiviral activity to in vivo concentration for prediction of antiviral effect: A critical step in treating COVID-19 patients. *Clin Infect Dis*. https://doi.org/https://doi.org/10.1093/cid/ciaa623.
29. Wang M, Cao R, Zhang L, et al. Remdesivir and chloroquine effectively inhibit the recently emerged novel coronavirus (2019-nCoV) in vitro. *Cell Res*. 2020;30:269-271.
30. Gordon DE, Jang GM, Bouhaddou M, et al. A SARS-CoV-2 protein interaction map reveals targets for drug repurposing. *Nature*. 2020;583:459-468.
31. Jeon S, Ko M, Lee J, et al. Identification of antiviral drug candidates against SARS-CoV-2 from FDA-approved drugs. *Antimicrob Agents Chemother*. 2020;64:e00819-e00820.
32. Zhou Q, Guo P, Kruh GD, Vicini P, Wang X, Gallo JM. Predicting human tumor drug concentrations from a preclinical pharmacokinetic model of temozolomide brain disposition. *Clin Cancer Res*. 2007;13:4271-4279.
33. Wang S, Zhou Q, Gallo JM. Demonstration of the equivalent pharmacokinetic/pharmacodynamic dosing strategy in a multiple-dose study of gefitinib. *Mol Cancer Ther*. 2009;8:1438-1447.

SUPPORTING INFORMATION

Additional supporting information may be found online in the Supporting Information section.

How to cite this article: Gallo JM. Hybrid physiologically-based pharmacokinetic model for remdesivir: Application to SARS-CoV-2. *Clin Transl Sci*. 2021;14:1082–1091. https://doi.org/10.1111/cts.12975